# Influence of Doping Level on Brillouin Oscillations in GaAs

Adam Dodson,[1,†] Andrey Baydin,[1,*,†,‡] Hongrui Wu,[1] Halina Krzyzanowska,[1,2] and Norman Tolk[1]

[1] *Department of Physics and Astronomy, Vanderbilt University, Nashville, Tennessee 37235, USA*

[2] *Institute of Physics, Maria Curie-Sklodowska University, Pl. M. Curie-Sklodowskiej 1, 20-031 Lublin, Poland*

(Received 16 August 2019; revised manuscript received 13 October 2019; published 4 November 2019)

Time-domain Brillouin scattering is a unique tool for determining depth-dependent material properties. Here, we show the influence of doping level in GaAs on Brillouin oscillations. Measurements are performed on intrinsic, *n*-type, and *p*-type GaAs samples. The results show high sensitivity of the amplitude of Brillouin oscillations to the doping concentration. Theoretical calculations are in good agreement with experimental data. This work provides an insight into specific dopant profiling as a function of depth.

DOI: 10.1103/PhysRevApplied.12.054006

## I. INTRODUCTION

Time-domain Brillouin scattering (TDBS) is an ultrafast pump-probe experimental technique based on the generation and detection of coherent acoustic phonons (CAPs). The inhomogeneous absorption of a pump pulse (<1 ps) in a material generates a CAP or strain wave in the order of nanometers that traverses the material [1]. The traveling CAP wave locally perturbs optical constants of the host. Thus, the reflection and transmission of an optical probe pulse that is delayed with respect to the pump pulse is modulated by the CAP wave. Interference of the probe light waves reflected from the surface of the material and from the traveling CAP wave results in oscillatory time-dependent signals referred to as Brillouin oscillations. Their amplitude, frequency, and decay are highly sensitive to optical and elastic properties of a material that, in principle, can be depth dependent [2].

TBDS is an invaluable tool to study different depth-dependent properties of materials [2,3], such as elastic and optical inhomogeneities in disordered films [4–6], ion-implantation-induced modification of interfacial bonding [7], sub-$\mu$m textures in materials compressed at megabar pressures [8,9], doping profiles [10], depth-dependent stress [11], imaging of grain microstructure [12,13], and determination of laser-induced temperature gradients in liquids [14]. TDBS is sensitive to ion-implantation-induced damage in gallium arsenide [15–17], diamond [18], and silicon carbide [19] at low fluences.

Here, we report on the influence of doping level in GaAs on Brillouin oscillations. Our experiment is carried out at probe energies near the band gap of GaAs for three samples: intrinsic, *n*-type, and *p*-type. The experimental results are also compared with a theoretical model developed in our earlier study [20]. Previously published research on the influence of doping profiles on CAP detection and generation shows that the doping profile, the position of the interface between differently doped regions, and the thickness of the transition region can be determined [10]. Contrary to this report, we investigate the probe energy region near the band gap of GaAs and show a qualitatively different way of determining doping concentrations. While another report has shown that the phase of Brillouin oscillations is sensitive to the doping level [21], we focus mainly on the amplitude of Brillouin oscillations. Moreover, we discuss that TDBS can be sensitive to both the doping concentration and the type of doping.

## II. RESULTS AND DISCUSSION

Samples of GaAs (100) grown by means of molecular beam epitaxy used in experiments are purchased from the Institute of Electronic Materials Technology, Warsaw, Poland. A total of three samples are studied: intrinsic, *n*-type, and *p*-type. The doping densities for those of *n*-type (Te) and *p*-type (Zn) are $1.28 - 2.35 \times 10^{18}$ cm$^{-3}$ and $2.94 \times 10^{19}$ cm$^{-3}$, respectively. A Ti layer (19 nm) is deposited onto all samples using an e-beam evaporator for efficient generation of CAPs. Ti is chosen due to its acoustic impedance, which matches that of GaAs with less than 10% mismatch and, therefore, acoustic reflections are suppressed at the Ti-GaAs interface.

TDBS experiments are performed in a standard time-resolved pump-probe setup in reflection geometry. A Coherent Mira 900 with 150 fs pulses at 76 MHz is used as a laser source. The wavelength of the laser varies between 825 nm and 900 nm. Both beams are focused onto the specimen with spot diameters of 100 $\mu$m and 80 $\mu$m for pump

*andrey.baydin@rice.edu

†These authors contributed equally to this work.

‡Present address: Department of Electrical and Computer Engineering, Rice University, Houston, Texas 77005, USA.

 © 2019 American Physical Society

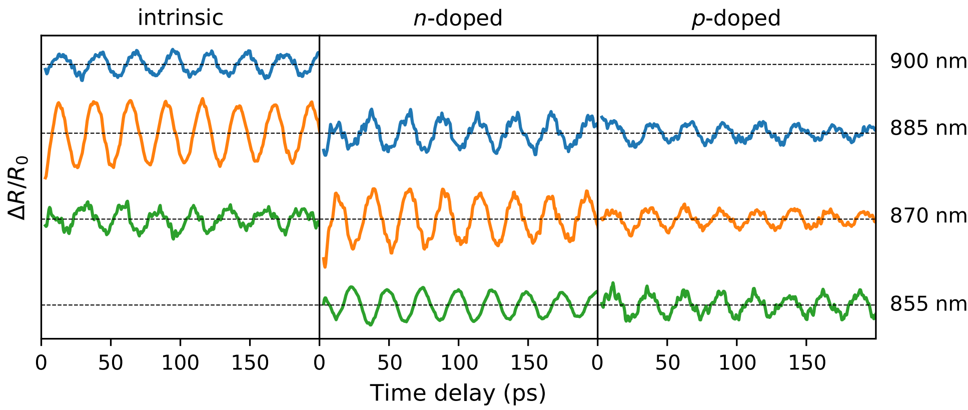


FIG. 1. Brillouin oscillations for intrinsic, $n$-type Te-doped ($1.28-2.35\times10^{18}$ cm$^{-3}$), and $p$-type Zn-doped ($2.94\times10^{19}$ cm$^{-3}$) GaAs at different probe wavelengths.

and probe, respectively. The pump beam is chopped using a Thorlabs optical chopper operating at 3 kHz.

Figure 1 shows representative Brillouin oscillations measured for intrinsic, $n$-type Te-doped ($1.28-2.35\times10^{18}$ cm$^{-3}$), and $p$-type Zn-doped ($2.94\times10^{19}$ cm$^{-3}$) GaAs at several probe wavelengths.

The thermal background due to excited carriers in the Ti layer is subtracted. The differences in experimental spectra for three samples are clearly seen in the amplitude of Brillouin oscillations. The amplitude changes as a function of probe wavelength for intrinsic and $n$-typeGaAs, whereas it is constant for $p$-type GaAs over the probed wavelength range. The frequencies of Brillouin oscillations for the studied samples are shown in Fig. 2. The frequency dependence is well described by the equation $f=2\sqrt{n^2-\sin^2\theta}vE_{\text{probe}}$, where $\theta$ is an angle of incidence of the probe beam (30°), $v$ is the longitudinal speed of sound, $n$ is the index of refraction of GaAs, and $E_{\text{probe}}$ is the probe energy. The index of refraction is measured by ellipsometry for all samples. The changes in frequency with respect to doping concentration are negligible and are not discussed further here.

The amplitudes of Brillouin oscillations as a function of probe wavelength for different doping levels are plotted in Fig. 3. As shown before [22], the amplitude of Brillouin oscillations changes drastically near the band edge and is maximized at the band gap (Γ point). Such dependence can be explained by the sharpness of the band edge. It has been shown in the case of GaP that the energy dependence of the amplitude of Brillouin oscillations, $A_{\text{osc}}$, agrees well with the derivative of the dielectric function [20].

$$A_{\text{osc}}\propto\left|\frac{\partial\epsilon}{\partial E}\right|=\sqrt{\left(\frac{\partial\epsilon_r}{\partial E}\right)^2+\left(\frac{\partial\epsilon_i}{\partial E}\right)^2},\qquad(1)$$

where $\epsilon$ is the dielectric function and $\epsilon_r$ and $\epsilon_i$ are the real and imaginary parts of the dielectric function, respectively. $E$ is the probe energy. Therefore, as observed in Fig. 4, which shows the dielectric function of GaAs, when one takes the derivative of the dielectric function, it is maximized near the band gap energy, since the slope in this region is steep. To match the scale of experimental data, all theoretical curves (the derivatives) are multiplied by the same factor, which includes the photoinduced strain magnitude and other experimental parameters that are, to a good degree of approximation, constant with respect to the probe energy.

For the $n$-type GaAs sample, the peak in the amplitude of Brillouin oscillations shifts to higher energies (shorter wavelengths) and broadens. While, for the $p$-type GaAs sample, no dependence of the amplitude of Brillouin oscillations on probe energy is observed in the probe energy region. Notably, in our case, the $p$-type sample has a higher concentration of carriers than that in the $n$-type sample. The response of the $n$- and $p$-type samples also agrees well with the predicted energy dependence based on the derivative of the dielectric function. As dopants are added to the GaAs lattice, donor or acceptor states, depending on the type of doping, form near the conduction or valence bands, respectively. This formation of dopant states results in changes in the dielectric function, such as smearing of the band edge for the imaginary part of the dielectric function [see Fig. 4(b)] and shifting and broadening of the peak associated with the band gap for the real part of the dielectric function [see Fig. 4(a)].

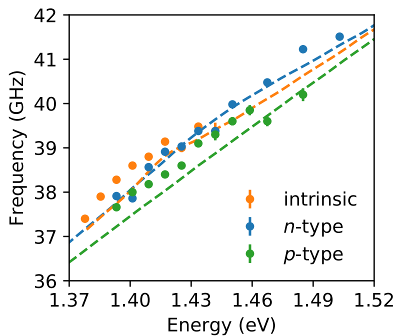


FIG. 2. Frequencies of Brillouin oscillations as a function of probe wavelength for intrinsic, $n$-type Te-doped ($1.28-2.35\times10^{18}$ cm$^{-3}$), and $p$-type Zn-doped ($2.94\times10^{19}$ cm$^{-3}$) GaAs. The dashed lines represent theoretical calculations. The error bars are in the order of the marker size.

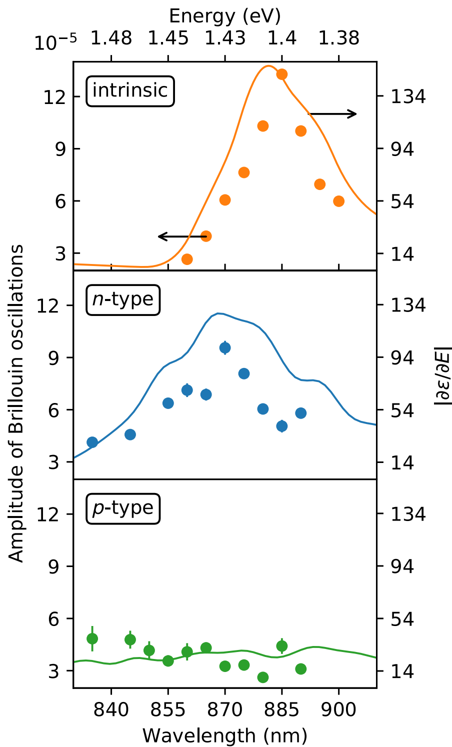


FIG. 3. Amplitudes of Brillouin oscillations as a function of probe wavelength for intrinsic, $n$-type Te-doped ($1.28 - 2.35 \times 10^{18}$ cm$^{-3}$), and $p$-type Zn-doped ($2.94 \times 10^{19}$ cm$^{-3}$) GaAs. The experimental data (dots) is compared to the theoretical model (lines). The error bars are in the order of the marker size.

Our results demonstrate that TDBS can be used to distinguish between different dopant concentrations. Although there are other techniques to measure doping levels, TDBS can uniquely provide depth resolution simultaneously with doping concentration.

As mentioned earlier, our $n$- and $p$-type samples have different doping concentrations. To gain some insight into how the type of doping affects the TBDS response, we take the dielectric functions for several doping concentrations from previous studies [23,24]. Figure 5 shows the derivative of the dielectric functions for $n$- and $p$-type GaAs at different doping concentrations. According to these theoretical estimations, the peaks for the $p$-type

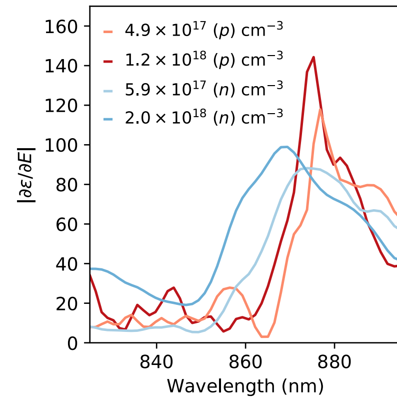


FIG. 5. Derivative of the dielectric function for different doping types and concentrations. The dielectric function is taken from Casey *et al.* [23,24].

sample are higher and narrower than those for $n$-type GaAs. This indicates that TDBS can be sensitive to both the doping concentration and the type of doping.

## III. CONCLUSION

We investigate the influence of the type and level of doping in GaAs on Brillouin oscillations using TDBS. The experiments are carried out for intrinsic, $n$-type, and $p$-type GaAs samples. The amplitude of Brillouin oscillations changes with respect to dopant level, while the change in their frequency is negligible. The energy dependence of the amplitude of Brillouin oscillations is well explained by the theoretical model based on the derivative of the dielectric function. Our results show that TDBS can be used to measure dopant concentrations. This report on the energy dependence of Brillouin oscillations adds another approach for the application of TBDS to nanoscale imaging. Particularly, we envision that TDBS spectra taken for a range of probe energies near direct optical transitions can be used to measure specific dopant concentrations as a function of depth. For example, applications can include monitoring wafer doping homogeneity with respect to depth, or determining the position and interface between different doping levels and types. Because various

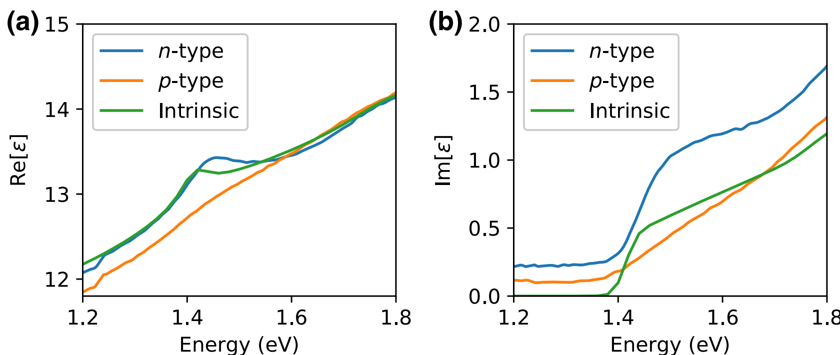


FIG. 4. Real (a) and imaginary (b) parts of the dielectric function for intrinsic , $n$-type Te-doped ($1.28 - 2.35 \times 10^{18}$ cm$^{-3}$), and $p$-type Zn-doped ($2.94 \times 10^{19}$ cm$^{-3}$) GaAs obtained using ellipsometry.

types of defects and impurities have different effects on the dielectric function, it should be possible to distinguish them and monitor their depth distributions. This is especially relevant for understanding the degradation of devices operating under harsh environments that are subject to radiation damage, as well as for defect inspection in semiconductor wafer metrology.

## ACKNOWLEDGMENTS

The authors acknowledge the ARO for financial support under Grant No. W911NF14-1-0290. Portions of this work has been completed using the shared resources at the Vanderbilt Institute of Nanoscale Science and Engineering (VINSE) core laboratories.

[1] C. Thomsen, H. T. Grahn, H. J. Maris, and J. Tauc, Surface generation and detection of phonons by picosecond light pulses, Phys. Rev. B **34**, 4129 (1986).

[2] V. E. Gusev and P. Ruello, Advances in applications of time-domain brillouin scattering for nanoscale imaging, Appl. Phys. Rev. **5**, 031101 (2018).

[3] A. Baydin, H. Krzyzanowska, L. Feldman, and N. Tolk, Post-implantation depth profiling using time-domain brillouin scattering, Nucl. Instrum. Methods Phys. Res., Sect. B: Beam Interact. Mater. At. **440**, 36 (2019).

[4] C. Mechri, P. Ruello, J. M. Breteau, M. R. Baklanov, P. Verdonck, and V. Gusev, Depth-profiling of elastic inhomogeneities in transparent nanoporous low-k materials by picosecond ultrasonic interferometry, Appl. Phys. Lett. **95**, 091907 (2009).

[5] V. Gusev, A. M. Lomonosov, P. Ruello, A. Ayouch, and G. Vaudel, Depth-profiling of elastic and optical inhomogeneities in transparent materials by picosecond ultrasonic interferometry: Theory, J. Appl. Phys. **110**, 124908 (2011).

[6] A. M. Lomonosov, A. Ayouch, P. Ruello, G. Vaudel, M. R. Baklanov, P. Verdonck, L. Zhao, and V. E. Gusev, Nanoscale noncontact subsurface investigations of mechanical and optical properties of nanoporous low-k material thin film, ACS Nano **6**, 1410 (2012).

[7] G. Tas, J. J. Loomis, H. J. Maris, A. A. Bailes, and L. E. Seiberling, Picosecond ultrasonics study of the modification of interfacial bonding by ion implantation, Appl. Phys. Lett. **72**, 2235 (1998).

[8] S. M. Nikitin, N. Chigarev, V. Tournat, A. Bulou, D. Gasteau, B. Castagnede, A. Zerr, and V. E. Gusev, Revealing sub-$\mu$m and $\mu$m-scale textures in $H_2O$ ice at megabar pressures by time-domain Brillouin scattering, Sci. Rep. **5**, 9352 (2015).

[9] M. Kuriakose, S. Raetz, N. Chigarev, S. M. Nikitin, A. Bulou, D. Gasteau, V. Tournat, B. Castagnede, A. Zerr, and V. E. Gusev, Picosecond laser ultrasonics for imaging of transparent polycrystalline materials compressed to megabar pressures, Ultrasonics **69**, 259 (2016).

[10] F. Hudert, A. Bartels, T. Dekorsy, and K. Köhler, Influence of doping profiles on coherent acoustic phonon detection and generation in semiconductors, J. Appl. Phys. **104**, 123509 (2008).

[11] J. Dai, P. Mukundhan, C. Kim, and H. J. Maris, Analysis of a picosecond ultrasonic method for measurement of stress in a substrate, J. Appl. Phys. **119**, 105705 (2016).

[12] M. Khafizov, J. Pakarinen, L. He, H. Henderson, M. Manuel, A. Nelson, B. Jaques, D. Butt, and D. Hurley, Subsurface imaging of grain microstructure using picosecond ultrasonics, Acta Mater. **112**, 209 (2016).

[13] Y. Wang, D. H. Hurley, Z. Hua, G. Sha, S. Raetz, V. E. Gusev, and M. Khafizov, Nondestructive characterization of polycrystalline 3D microstructure with time-domain brillouin scattering, Scr. Mater. **166**, 34 (2019).

[14] I. Chaban, D. Shin, C. Klieber, R. Busselez, V. Gusev, K. A. Nelson, and T. Pezeril, Time-domain Brillouin scattering for the determination of laser-induced temperature gradients in liquids, Rev. Sci. Instrum. **88**, 074904 (2017).

[15] A. Steigerwald, Y. Xu, J. Qi, J. Gregory, X. Liu, J. K. Furdyna, K. Varga, A. B. Hmelo, G. Lüpke, L. C. Feldman, and N. Tolk, Semiconductor point defect concentration profiles measured using coherent acoustic phonon waves, Appl. Phys. Lett. **94**, 111910 (2009).

[16] A. Steigerwald, A. B. Hmelo, K. Varga, L. C. Feldman, and N. Tolk, Determination of optical damage cross-sections and volumes surrounding ion bombardment tracks in GaAs using coherent acoustic phonon spectroscopy, J. Appl. Phys. **112**, 013514 (2012).

[17] A. Baydin, H. Krzyzanowska, R. Gatamov, J. Garnett, and N. Tolk, The photoelastic coefficient $P_{12}$ of $H^+$ implanted GaAs as a function of defect density, Sci. Rep. **7**, 15150 (2017).

[18] J. Gregory, A. Steigerwald, H. Takahashi, A. Hmelo, and N. Tolk, Ion implantation induced modification of optical properties in single-crystal diamond studied by coherent acoustic phonon spectroscopy, Appl. Phys. Lett. **101**, 181904 (2012).

[19] A. Baydin, H. Krzyzanowska, M. Dhanunjaya, S. V. S. N. Rao, J. L. Davidson, L. C. Feldman, and N. H. Tolk, Depth dependent modification of optical constants arising from $H^+$ implantation in $n$-type 4H-SiC measured using coherent acoustic phonons, APL Photonics **1**, 036102 (2016).

[20] A. Baydin, R. Gatamov, H. Krzyzanowska, C. J. Stanton, and N. Tolk, Energy-dependent amplitude of brillouin oscillations in gap, Phys. Rev. B **99**, 165202 (2019).

[21] P. Babilotte, E. Morozov, P. Ruello, D. Mounier, M. Edely, J.-M. Breteau, A. Bulou, and V. Gusev, in *Journal of Physics: Conference Series* (IOP Publishing, 2007), Vol. 92, p. 012019.

[22] J. K. Miller, J. Qi, Y. Xu, Y.-J. Cho, X. Liu, J. K. Furdyna, I. Perakis, T. V. Shahbazyan, and N. Tolk, Near-bandgap wavelength dependence of long-lived traveling coherent longitudinal acoustic phonons in GaSb-GaAs heterostructures, Phys. Rev. B **74**, 113313 (2006).

[23] H. C. Casey, D. D. Sell, and K. W. Wecht, Concentration dependence of the absorption coefficient for $n$- and $p$-type GaAs between 1.3 and 1.6 eV, J. Appl. Phys. **46**, 250 (1975).

[24] D. Sell, H. Casey, Jr, and K. Wecht, Concentration dependence of the refractive index for $n$- and $p$-type GaAs between 1.2 and 1.8 eV, J. Appl. Phys. **45**, 2650 (1974).